Iraqi Journal of Science, 2026, Vol. 67, No. 2, pp: 927-952
DOI: 10.24996/ijs.2026.67.2.26

ISSN: 0067-2904

Impact of Post-Stack Seismic Inversion on Volumetric Estimation in Pliocene Channel Reservoirs: A Case Study from the Nile Delta's Baltim Field

Ali Saeed Ali EL-SAYED*, Walid M. MABROUK, Ahmed M. METWALLY
Geophysics Department, Faculty of Science, Cairo University, Giza, 12613, Egypt

Received:28/ 4/2024 Accepted: 9/ 2 /2025 Published: 28/2/2026

Abstract

This study addresses the challenge of identifying Pliocene reservoir channels where small quantities of hydrocarbons can cause misleading Class III AVO anomalies, leading to inaccurate predictions of commercially unviable gas. It explores whether seismic attributes, such as far amplitude, in combination with well-log data, can confirm the presence of a prospective anomaly. This is especially relevant for the Kanaria Pliocene feature within the Baltim North area, offshore in the Nile Delta. To investigate this, we employed a range of post-stack seismic inversion techniques, including colored inversion, sparse spike inversion, band-limited inversion, and model-based inversion, to delineate the hydrocarbon-rich sands in the Kanaria Pliocene sand channel. Petrophysical data from five wells (BN-3, BNE-17dir, ANDALLEB-1, TERSA-1 ST, and WB-1) were incorporated to support the analysis. Results revealed low acoustic impedance sands at both the top and base of the Kanaria Pliocene feature. The sandstones from the BN-3 and BNE-17dir wells showed significant potential, with an average shale volume of 33%, total porosity of 26%, effective porosity of 21%, and hydrocarbon saturation of 40%. Using post-stack seismic inversion, particularly color inversion (with a correlation of 0.98) and band-limited inversion (with a correlation of 0.96), the study improved the estimation of gas initially in place (GIIP). Gas in place for the Pliocene reservoirs was estimated to increase from 32.87 billion standard cubic feet (BCF) to 33.93 billion standard cubic feet (BSCF), confirming the presence of a promising anomaly and enhancing the potential for successful drilling and future development. This confirmation opens the possibility for exploration and development wells in the future.

Keywords: Post-stack inversion, hydrocarbon-rich sands, Baltim North, offshore Nile Delta, Pliocene reservoirs.

Abbreviations:

- Nile Delta: ND
- Abu Madi: A.M.
- Kafr El Sheikh: K.F.
- Formation: Fm.
- Baltim Gas Field: BGF
- Pliocene Prospective anomaly: P.P.A.
- Sandstone reservoirs: S.S.R.
- Acoustic impedance: AI

*Email: aliyehia665@yahoo.com

تاثير الأنعكاسات السيزميه بعد التجميع على التقديرات الحجمية لقنوات البليوسين، حقل غاز بلطيم، دلتا النيل مصر

على سعيد على السيد*, وليد محمد مبروك, أحمد محسن متولى

قسم الجيوفيزياء ، كلية العلوم ، جامعة القاهره، الجيزة، مصر

الخلاصة

إن المشكلة الأساسية التي حلتها هذه الدراسة هي السعة الوهمية التي يمكن أن تظهر على أساس وجود كمية ضئيلة من الغاز والتي تعتبر غير تجارية للإنتاج، وهو ما يجعل التقييد بالحفر لتجنب أي انخفاض في إمكانية نجاح الحفر، لذا فإن المساهمة الأساسية لهذا البحث هي تنفيذ أنواع مختلفة من الانقلاب ما بعد المكدس، وتحديدًا الانعكاسيه الملونة والمحدودة النطاق، والتي تعطي ممانعة صوتية منخفضة في رمال مكمن الغاز البليوسين العلوي ثم مقارنة النتائج مع الخصائص الزلزالية كخاصية السعة، والتي تعطي حجمًا كبيرًا في السعة البعيدة مقارنة بالحجم المنخفض للسعة القريبة، مما يعطي مؤشرًا للفئة الثالثة من السعة مقابل الإزاحة (AVO)، وبالتالي زادت قيمة الغاز في البداية (GIIP) من 32.87 مليار قدم مكعب قياسي (BSCF) إلى 33.93 مليار قدم مكعب مبتذل (BSCF). بعد ذلك، من خلال تنفيذ طرق مختلفة للانعكاس بعد التكديس على مكعب زلزالي، يتم إنتاج مكعبات انعكاس زلزالية متميزة. ومن بين هذه العناصر، أثبت مكعب الانعكاس الملون بعد الكدس ومكعب الانعكاس بعد الكدس ذي النطاق المحدود أنهما الأكثر فائدة لتقدير حجم الغاز، وبالتالي تعزيز إمكانية نجاح احتمال البليوسين في منطقة حقل بلطيم. وسيشجع هذا النجاح على حفر المزيد من آبار الغاز، مما يؤدي إلى زيادة إنتاج الغاز في منطقة حقل بلطيم.

1. Introduction

Early in the 1960s, the Nile Delta basin showed signs of having hydrocarbon potential; trillions of cubic feet of gas were found [1]. This incredible gas province covers various stratigraphic stages, including the Oligocene, Pliocene, and Pleistocene. Notable scholars [2], [3], [4], [5], [6], [7], [8], [9], [10], [11], have all recognized the significance of this finding: The Baltim gas fields are situated in the offshore area of the Nile Delta, which was discovered in 1995 by well Baltim North-01 and in 1993 by well Baltim East-01. Baltim North currently has seven wells drilled, whereas Baltim East has twelve with enormous gas condensate accumulations [12], the offshore Nile Delta is currently developing into a significant gas field. High-resolution three-dimensional (3-D) seismic data and information gathered from thirteen sequential successful deep-water explorations and appraisal wells to recognize different sediment deposition and erosion stages inside deep-marine slope channels during the uppermost Pliocene effectively utilized [13]. The field is termed "Kafr EL Sheikh (K.F.)," from the early to late Pliocene age. The northern region of the central portion of the sub-basin is known as the Baltim fields, which contain most of the gas fields in the Baltim area. This sub-basin contains a thick marine succession of sediments from the Mid-Late Tertiary period, located beneath the deltaic deposits of the current Nile Delta area. Baltim gas fields are fault-bounded in the north and south and feature shale out against incised valley slopes. These are stratigraphic and structural combination traps. There are two primary sandstone reservoirs (S.S.R.) from which gas and condensate are produced.

This study's primary goal is to verify that hydrocarbons were present in Pliocene gas-bearing sand for the K.F. formation's channel. Applying various post-stack inversions, especially different seismic attributes as amplitude, can give a fake response for gas existence due to a tiny amount of gas as a huge amount of gas, which can't give a commercial gas-bearing reservoir. Seismic inversion findings are presented as distinct cubes, including

impedance and geological features. These results are important for identifying potential energy accumulations along with structural characteristics, and this inversion process involves estimating model parameters, specifically impedance, instead of reflectivity [14], [15], [16], [17]. This is achieved by converting seismic reflection amplitude into an impedance profile, which provides data about the rock's properties. The objective is to reduce the disparities within the observed and simulated seismic data by employing the inversion approach [18], [19], the main goal is to improve lithology and fluid prediction, as well as prospect delineation, by extracting the geological background and reservoir characteristics from a particular set of recorded seismic data. The objective is to minimize the disparities between the recorded and modelled seismic data USING the inversion approach [18].

An additional three studies have been conducted in the Nile Delta region. The first, by Metwally et al. [50], assesses hydrocarbon potential across the Abu Madi (A.M.) Formation (Fm.) within the Baltim gas field (BGF), utilizing petrophysical analysis and well data to enhance reservoir quality. The second, by El-Mowafy [13], applies AVO analysis to detect Pliocene channelized gas sands in the Scarab field, aiding in identifying new reserves. The third study, by Othman [20], employs probabilistic neural network (PNN) analysis combined with post-stack inversion to forecast shale volume and predict gas reserves in the Sapphire gas field.

The key distinction between these earlier studies and the present research is the focus on the shallow reservoir (Pliocene gas-bearing sand in the K.F. Fm.). This study utilizes post-stack inversion techniques, particularly colored and band-limited post-stack inversion, to delineate the gas-bearing sand channel of the Pliocene Prospective anomaly (P.P.A.). Three producing gas wells (BN-3, BNE-1 dir, and ANDALEEB-1) confirm high inversion analysis results and low acoustic impedance (AI) for the top gas sand reservoir. Moreover, the volume calculation increased with post-stack seismic inversion, expanding the gas area. Finally, after applying all variations of post-stack inversion, specially colored and band-limited post-stack inversion, which give good indication and delineation for the gas-bearing sand channel of the P.P.A., we also increased the initial gas in-place from 32.87 billion cubic feet (BCF) to 33.93 billion cubic feet (BCF). This enhances the assurance and volumetric calculation of potential anomalies, along with ascertaining the optimal position for the placement of wellbores within potential anomalies.

In conclusion, this study confirms the significant hydrocarbon potential of shallow Pliocene reservoirs in the Nile Delta, reinforcing previous research findings. The Nile Delta remains one of Egypt's largest and most productive petroleum regions, with substantial hydrocarbon reserves in both shallow and deep formations.

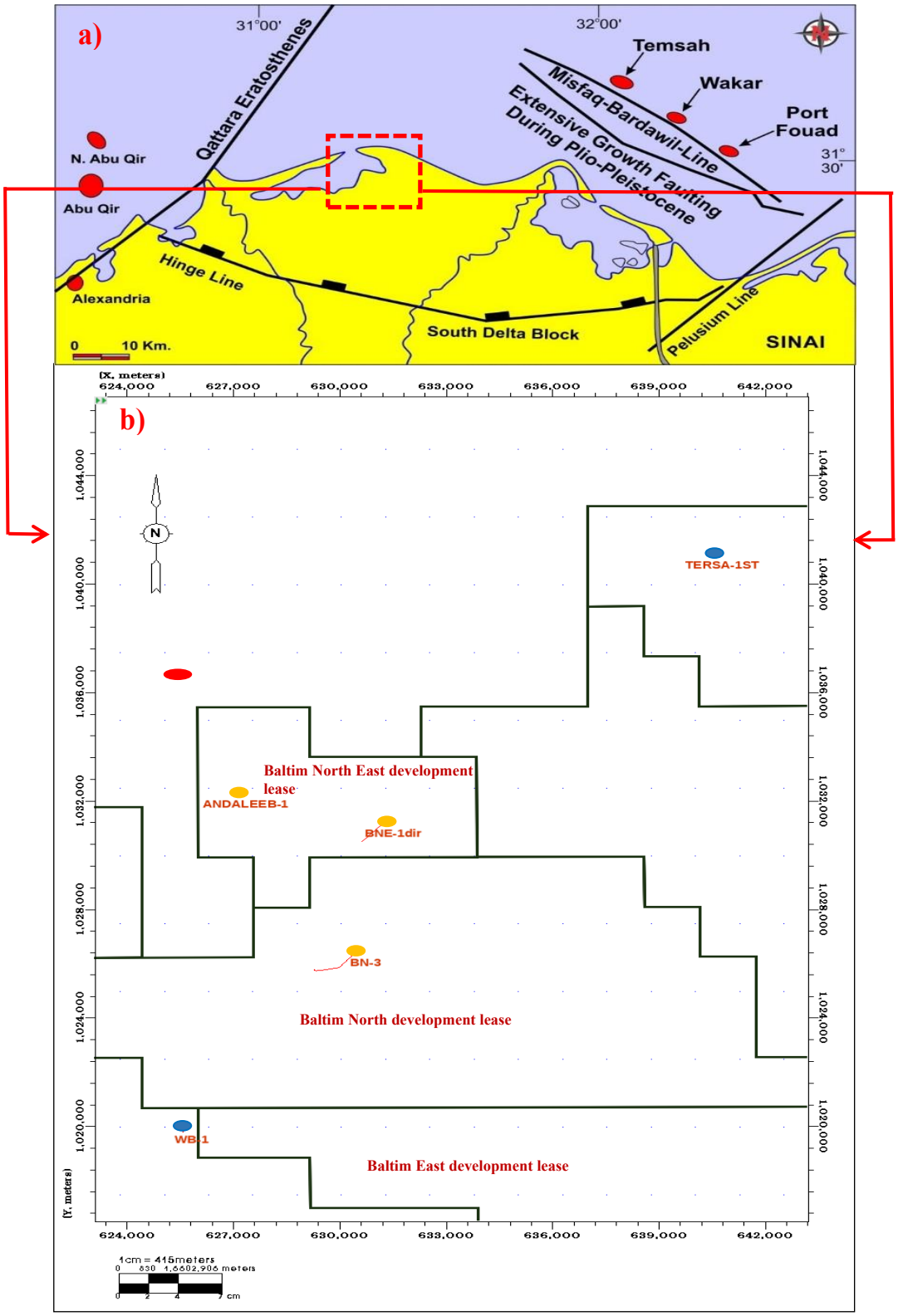

Figure 1: a) Nile Delta regional tectonic map [21]. b) Base map showing development leases and well locations, with 3D seismic survey represented by black dots.

2. Structure and stratigraphy of N.D

2.1 Structure setting

The deposits of the ND region have been shaped by several tectonic movements [22]. These events, along with eustatic changes, have been critical in controlling the amount of

sediment supplied to the valley and establishing the amount of accommodation space. Transpressional inversion occurred along the Tethyan rift boundary throughout the Jurassic to Early Cretaceous era. This episode, which included intermittent uplift periods, concluded in the late Eocene. This phenomenon causes deformation, which is primarily responsible for the Nile Delta's pre-Messinian structure. From the Late Eocene until the Oligocene, Egypt's tectonic tilt was northward into the Mediterranean, corresponding with the emergence of the Gulf of Suez [22], [30].

Major structural trends (Figure 1) govern the Nile Delta Structural Setting [23], [24], [25], [26], [27], [28], 29], [30], [31]. Hinge Zone of the Nile Delta: A substantial bend zone that divides the northern portion of the delta valley from the southern basin block at around 31° N. There is a significant throw down to the north on this group of nearly E-W trending faults with a significant northward throw [32].

The Hinge Zone splits the Delta further into the south Delta Block and the north Delta Basin. Beyond the Hinge Zone towards the north, there is a thick tertiary section that is at least 15,000 to 20,000 feet thick, while to the south (South Delta Block), it is 1,500 to 5,000 feet thick. Apart from its structural attributes, the Hinge line denotes a significant facies transition boundary between the platform and slope carbonates.

- *The Rosetta Trend:* The Qattara-Eratosthenes trend creates a significant structural relief, resulting from the lateral displacement of rocks along the Qattara-Eratosthenes (Rosetta) fault, which extends in a northeast-southwest orientation, highlighting the clear evidence of this phenomenon. The source rock, situated atop deepwater sediments from the Late Cretaceous to Early Tertiary period, strongly suggests that the fault displacement is closely associated with the Late Cretaceous. This fault system, remarkable in its own right, shows evidence of activity extending from the early Miocene to the late Pleistocene.
- *El Temsah Trend:* The fault trend known as Misfaq-Bardawil (Temsah) comprises numerous parallel NW-SE faults that extend east. Parallel to this trend, the oblique sinking of Africa via the Cyprus trench was linked to the appearance of Pliocene wrench fault activity, where *these* faults appear to have triggered salt movement (pillows to diapirism) throughout the Pliocene. During the Middle Miocene, the right-lateral oblique-slip trend influenced the Temsah trend. The NW Damietta concession is situated northeast of this significant oblique-slip fault. Conjugated fault trends, the Temsah dextral slip and the Rosetta sinistral slip are found in the Ultra-Deep Marine. They were renewed during the Neogene and are inherited from the Mesozoic rifting [3in the Late Cretaceous period.
- *Baltim Trend:* A *sequence* of North to South faults developed throughout the late Eocene to recent tectonic ages. It was developed during the Early Miocene when the pre-Tertiary structure was rejuvenated.

2.2 General stratigraphy of Nile delta

The Nile Delta Basin underwent a significant retreat during the upper Miocene, similar to the rest of the Mediterranean. Evaporitic sediments originated in the Rosetta Fm.as as a result of erosion. Whereas deep incised valleys witnessed fluvial deposition through marginal marine facies, generating the A.M. Fm. (Figure 2). During the Late Pliocene, the rising sea levels generated a broad transgression, elevating bathyal facies over the formerly limited Messinian units across the coastal shelf. In the Lower Pliocene, the sea level rose, resulting in a broad transgression that transported bathyal facies over the previously confined Messinian units throughout the continental margin.

Progradation is the most noticeable characteristic of the plio-Plioestocene deposits of the Nile delta, combined with huge clinoforms with a significant northern shift in the shelf break. Nevertheless, there were also occurrences of backward phases.

The Plio-Pleistocene section's surfaces were shaped in marine environments ranging from shallow to open. Distinguishing between these surfaces is possible due to the movement of shelf sediments towards the north, resulting in turbidity flows that descend down the slope and into the basin. The extensive Pliocene of K.F. Fm. It comprises 98% shale clastic strata, which originated due to sediment inflow from the Nile Delta. In the K.F region of the Nile Delta, the reservoir facies largely consist of channel sands that are generally big and demonstrate a fining upward tendency [33]. The Plio-Pleistocene strata of the Nile Delta were laid down on a slope towards the basin floor. Extensive study on sequence stratigraphy has enabled the calibration of basin-fill models, which anticipate diverse turbidity conditions impacted by fault movement and mobile salt during deposition. Within this scenario, there is a cohabitation of multiple habitats. Along the strike, a graded slope exists where sheet sands can build in depressions created by faults. Additionally, unrestricted turbidity deposition occurs in slope channel systems, providing extensive data on most of the Nile Delta formations [34], [35]. The division of the Miocene series is as follows:

- *Sidi Salem Fm. (Serravallian Tortonian):* The Fm. of basins bordered by listric faults occurred during the Early Serravallian, a time of fast sea level decline and extensive tectonic activity in the eastern Mediterranean from 3592 to 4038 meters. The bottom sequence of the well Sidi Salem-1 is the type section of this unit. Sandstones and siltstones are sporadically interbedded with clays in the Fm., along with occasional dolomitic marls. Gray-green clays are mostly composed of kaolinite, along with illite and montmorillonite [35].
- *Qawasim Fm. (lower Messinian):* It comprises conglomerate strata and thick sandstone interbedded with clay, as shown in Qawasim well-1, which spans 2800 to 3733 meters [35].
- *A.M. Fm. (upper Messinian):* In the Abu A.M. Madi, El Qar'a, East Delta, Baltim, and Abu Qir fields in the central basin, the Fm. Serves as the primary hydrocarbon resource. The Qawasim and A.M. successions on top of it are truncated according to the dipmeter data. The type section may be found in the well Abu Madi-1 between 3007 and 3229 meters. It is characterized by several thick, pebbly sand bodies with thin shales interbedded throughout [35].
- *Rosetta Fm. (Messinian):* Thick layers of anhydrite and thin claystones interbedded essentially define the Rosetta Fm.. The Fm. was discovered in the borehole Rosetta-2 between 678 and 2718 meters. The occurrence of Rossetta anhydrite appears to be restricted to the Delta's offshore northern section [35].

The division of the Plio-Pleistocene series is as described below:

- *K.F. Fm. (Pliocene):* The composition comprises subaqueous continental incline shales that alternate with turbidite sands. The well Kafr El Sheikh-1 represents this section type, spanning from 1277 to 2735 meters [35].
- *El Wastani Fm. (Upper Pliocene):* The El Wastani Fm. has a thickness of 123 meters in the El Wastani-1 well, extending from 1009 to 1132 meters. This litho-stratigraphical unit consists of thick sandstones with interbeds containing clay minerals.

The depositional setting of this Fm. is the continental shelf [35].

- *Mit-Ghamr Fm. (Pleistocene):* The well Mit-Ghamr-1 encountered the Mit-Ghamr *Fm.* at depths ranging from 20 to 484 meters. The depositional setting of this Fm. can be described as fluvial to shallow marine, specifically the delta front [35]]. The Holocene epoch comprises the Bilqas Fm., which is the uppermost layer enveloping the Delta region and primarily comprises sandy and clayey sediments.

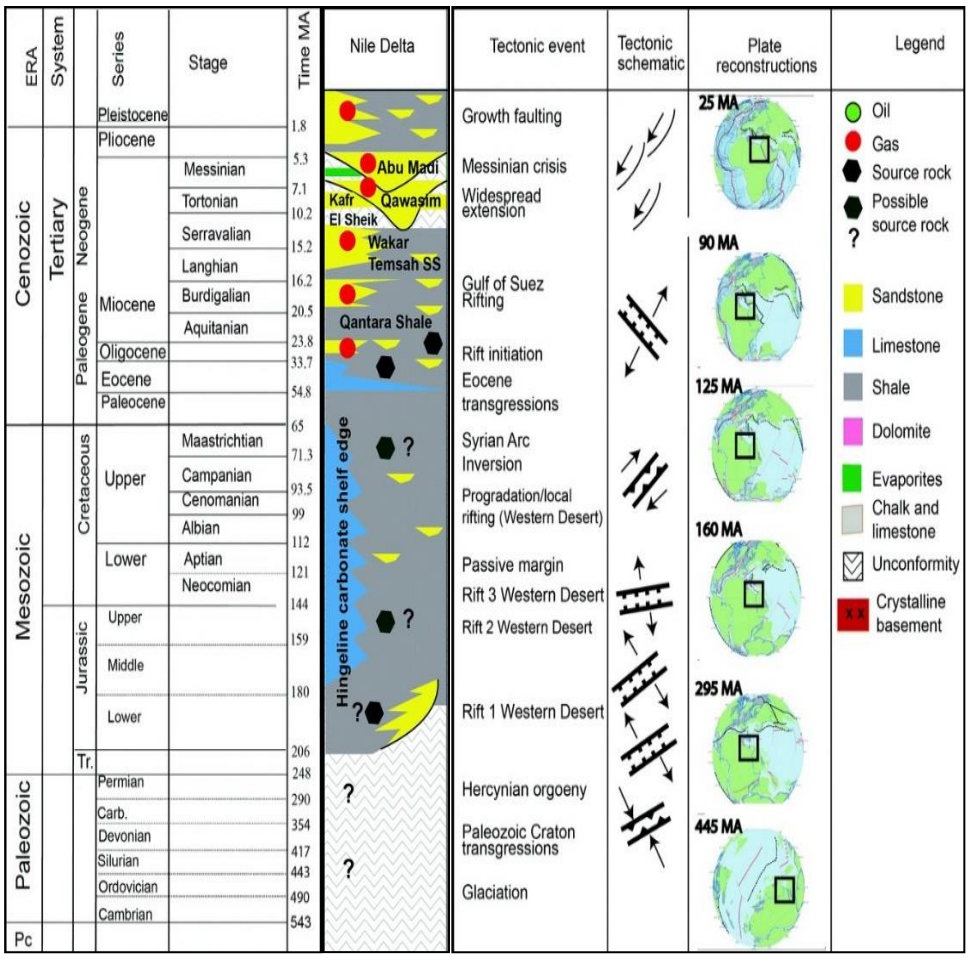

Figure 2: Nile Delta stratigraphic column (Dolson, 2019).

3. Available Data

This investigation systematically organizes all applicable data into a grid-like structure. Seismic interpretation in the study area is carried out using 3D full post-stack time migration (PSTM), also known as central processing, obtained in 2018. This data was integrated with information from five wells, aligned with the seismic grid established earlier to achieve the research objectives (Figure 1). Additionally, these wells utilize the available post-stack seismic data, referred to as the full stack. The primary focus of this work is to apply the full-stack data across various post-stack inversion techniques, thereby improving and refining the volumetric assessment and understanding of the Kanaria anomaly.

4. Methodology

Post-stack seismic inversion was utilized to calculate the amount of gas initially in place using integrated seismic and well-log data. Post-stack seismic inversion uses various classifications and algorithms, like colored and genetic inversion processes, to show reservoir properties more complexly [36], [37]. It also uses sparse spike inversion to find the locations of these noticeable spikes [49]. Band-limited inversion is the same approach as spectral decomposition, which transforms frequency domain data from time domain data [38], [39], and model-based inversion is a unique category of seismic inversion where well logs are used to produce a high-frequency initial geological model that is generated to understand the geological formations.

Impedance is not a geological property like a contact feature but can be understood in a geological setting [40]. Choosing the right inversion algorithm is important for characterizing

reservoirs using seismic data, especially in areas with complex geology [41]. Seismic inversion following stacking is a technique that transforms a migrated seismic volume with a zero offset and a full stack, converting it into an AI volume. This conversion is accomplished by adding well and seismic data, and important details about the stratigraphy and structure, all of which support the interpretation objective. Conversely, post-stack inversion techniques comprise a diverse range of procedures that are utilized to transform stacked seismic data into quantifiable attributes related to the physics of rocks [42], [43]. The final outcome of this inversion procedure is visible in the computation of P-impedance. The inversion analysis applies various frequency elements, from extremely low to high frequencies. The extremely low plus low-frequency components are produced using seismic velocity and drilling data, while high frequencies are incorporated from well data, and the frequency within a defined range is introduced using seismic data [44]. The initial stage in implementing post-stack seismic inversion involves establishing a correlation between the alignment of well data and seismic data, allowing the rocks' AI characteristics to be evaluated. To enhance the alignment between well data and seismic data, appropriate filters for frequency and time were utilized on the wavelets, resulting in a thorough analysis.

This study aims to identify a Pliocene gas channel within the K.F. Fm., specifically the Kanaria P.P.A. To achieve this, the study employs post-stack seismic inversion using various inversion types and a single velocity function derived from a time-depth plot. This function transforms the seismic data into a depth section and synthetic seismogram for time-domain interpretation. The inversion results confirm the presence of a gas prospective anomaly. They are integrated with volumetric calculations to estimate the Gas Initially in Place (GIIP), enhancing the potential for success in the Kanaria prospect. As outlined in the general workflow (Fig. 3), the seismic data is first transformed into inverted impedance after the stack inversion, which results in an updated gas area polygon based on the new inversion results, and this data is subsequently used for volumetric estimation.

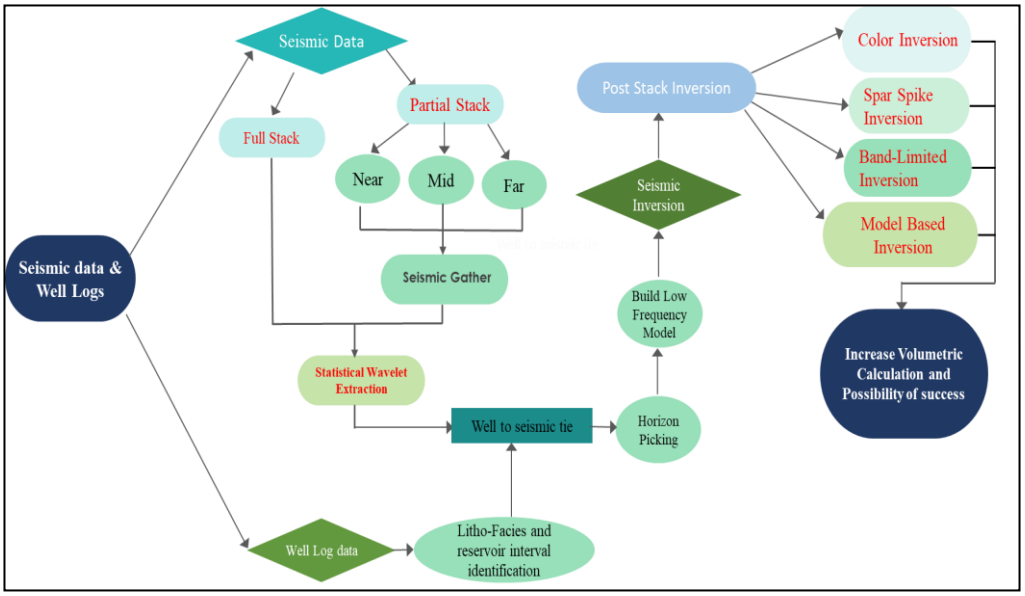

Figure 3: Research Workflow, From Seismic data till volumetric calculation.

5. Results and Discussion

This section displays the steps of post-stack inversion with different types to increase the volumetric calculation as the first step by utilizing seismic to well tie to identify and select the interpreted horizon for P.P.A. by employing a synthetic seismogram generated at BNE-1 dir and Andaleeb-1 for the second P.P.A. (K.F. Fm.). The second phase involves creating a

time grid for the P.P.A (K.F. Fm.) at the top gas sand reservoir. This grid is subsequently timed by an initial velocity operation of 2070 m/s obtained via the time-depth diagram. Consequently, a depth contour map with a depth range of 2300 to 2380 meters is the end product of the interpretation. The well is situated on a higher structure with a high far-amplitude anomaly (Fig. 4a) according to the contour map and a low near-amplitude anomaly (Fig. 4b), which is classified as Class III (Fig. 4).

6. Analysis and Interpretation

6.1 Petrophysical Analysis

Petrophysical assessment is a critical stage in calculating hydrocarbon reserves. The most essential stage in the evaluation of reservoir petrophysical parameters is well-log analysis, which includes porosity, shale content, water, and hydrocarbon saturation [45] [46], [47], [48], [49], [50]. The P.P.A (K.F. Fm.), which is mostly S.S.R., is utilized at two discovery wells to quantify the reservoir: the first well is Baltim north -3 (BN-3), with a true vertical depth between 2370 and 2383 m; BNE-1 dir (BNE-1 dir) measures a true vertical depth between 2496 and 2508 m. The presence of hydrocarbons in the reservoir is indicated by the clear crossover observed between density and neutron logs, which helps identify the porous zones. The petrophysical parameters were calculated using Techlog software, providing estimates for total porosity (PHIT) and effective porosity (PHIE) For the BNE-1 dir well, the average total porosity was 21%, effective porosity was 24%, and water saturation was 54%. For the BN-3 well, the average total porosity was 26%, effective porosity was 27%, and water saturation was 50% (refer to Table 1). These parameters are integral to the volumetric calculations used for hydrocarbon estimation, as shown in Fig. 5.

Table 1: Combined the petrophysical data utilized in the volumetric calculation for BN-3, BNE-1 dir, and Andaleeb-1 in the K.F. Fm. (P.P.A).

Parameters	*BALTIM NORTH -3 (BN-3)*	*Baltim NORTH East 1 dir BNE-1 dir*	*ANDALEEB-1*
Depth (m)	2370-2383	2496-2508	2644–2668
Gross Thickness (m)	15	13	24
Net Reservoir (m)	6	8	6
Net Pay (m)	5.5	4	3
Porosity (%)	26	21	28
Water Saturation (%)	50	54	53

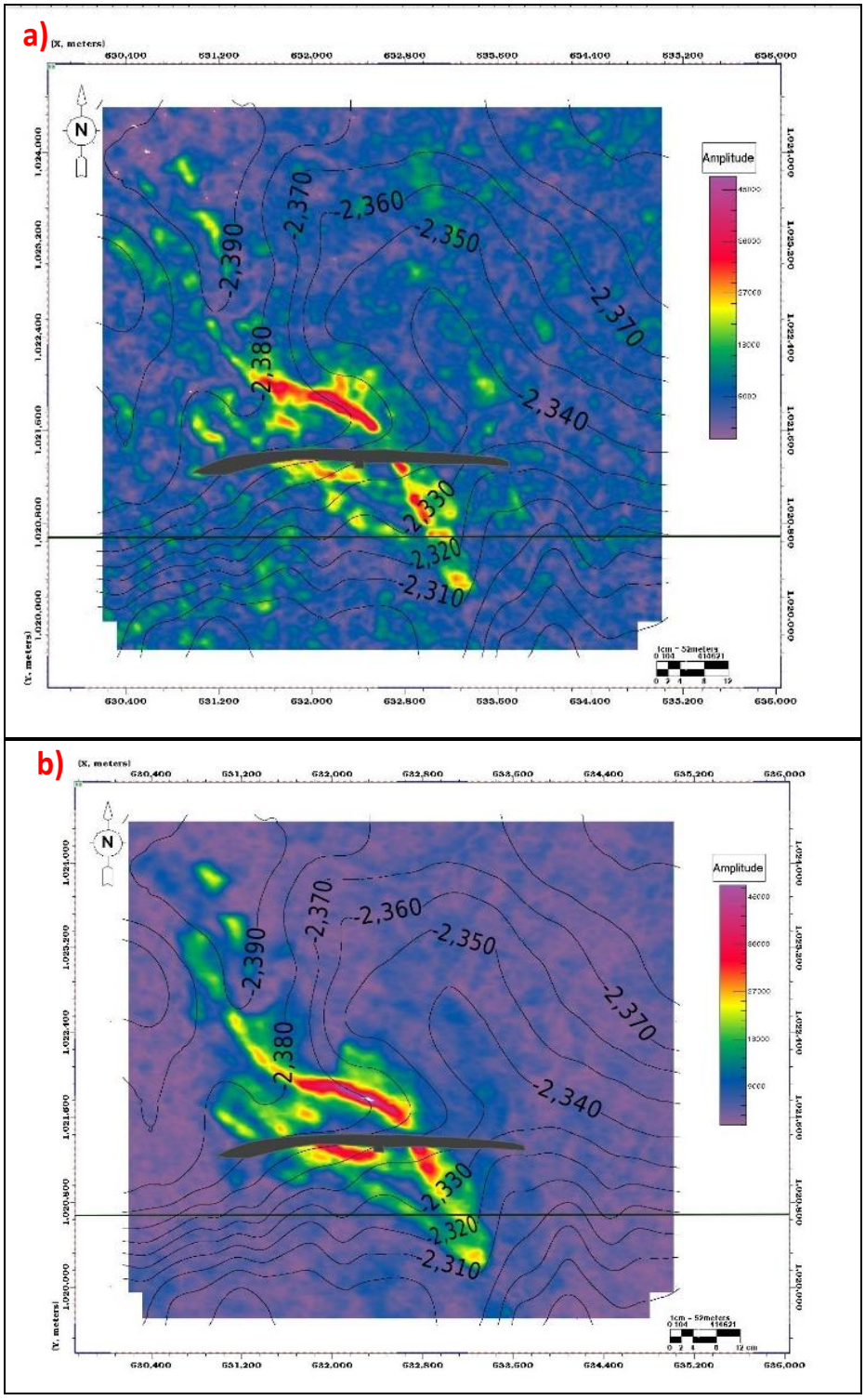

Figure 4: a) P.P.A., (-25, 50) ms, far structure amplitude Map, b) P.P.A., (-25, 50) ms, near structure amplitude Map.

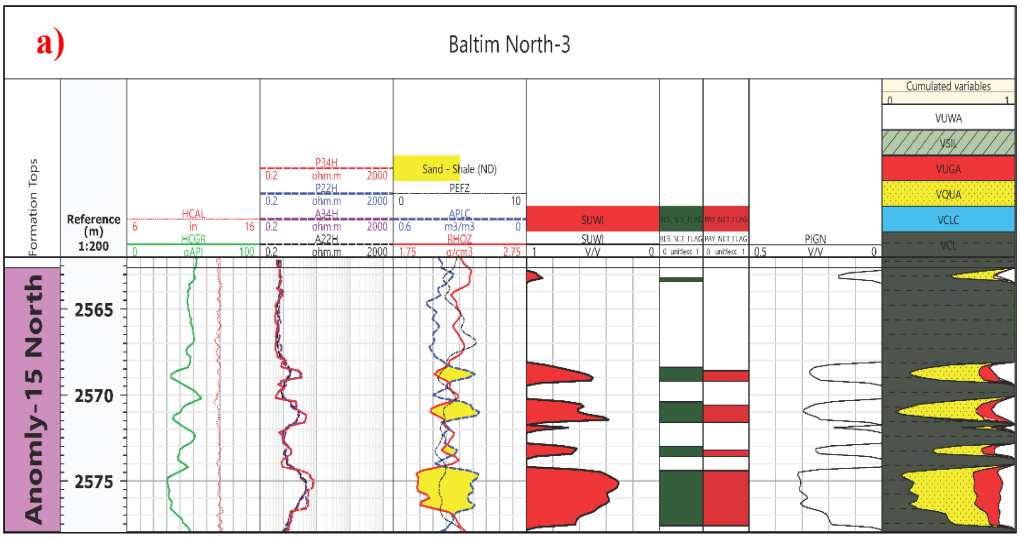

Figure 5 : a) Petrophysical interpretation of BALTIM North-3 (BN-3) well (Anomly-15 North), (K.F. Fm.) b) Petrophysical interpretation of BALTIM North East-1 dir (BNE-1 dir) well (Plio-1c), (K.F.Fm.)

6.2 Seismic inversion

Seismic inversion approaches employ well-logged data in conjunction with seismic potential to create fundamental models that coincide with the observable properties of rocks and fluids. It is crucial to realize that, even without well data, the properties related to lithology and fluids may still be derived from the inverted seismic data [51], [52], [53], as the next workflow phases.

1. Perform seismic to well tie and wavelet extraction.
2. Calculating shear velocity for wells whose velocity is not calculated by using the Greenberg-Castagna equation.
3. Fluid Substitution models all scenarios with different fluid subs. To reach the best petrophysical model.
4. Build an Initial model for all Post-stack inversion types.
5. Volumetric assessment.

6.2.1 Synthetic seismogram

Well-to-seismic correlation is an essential aspect of subsurface analysis that connects borehole measurements, recorded in depth, to seismic information presented in time, expressed in time units. This enables the identification of reservoir tops, such as the Pliocene sands, in seismic sections. AI is calculated by combining density and P-sonic data from the well logs. Reflectivity, or the reflection coefficient, can be derived from the AI [54]. To ensure accurate alignment, the calculated seismic trace is compared with composite seismic data gathered from the well path [55], [56], [57], [58], [59].

The P.P.A. in the K.F. Fm., identified as a gas-bearing sand reservoir, was observed as a positive high-amplitude reflector (soft-kick). The successful seismic ties confirm that the seismic data used in this study follows European polarity and zero phase. In this context, an increase in AI corresponds to negative amplitude values (troughs), while a decrease in impedance corresponds to positive amplitude values (peaks). The P.P.A. in the BNE-1 dir well, demonstrating significant correlation values of about 0.56%, is illustrated in Figures 6a ('Correlation of well and seismic data for BNE-1 dir well'), 6b ('Wavelet statistical properties for BNE-1 dir well'), and 6c ('Analysis of phase and signal polarity for BNE-1 dir well. The study's findings show the relationship between the seismic data and five analyzed wells.

By applying these parameters, the gas Initially in Place (GIIP) after applying seismic inversion to identify the best gas area for the hydrocarbon calculation increased at the P.P.A., where the mean gas area increased from 3.10 Km^2 to 3.68 Km^2, and the mean value of gas Initially in Place (GIIP) changed from around 0.93 Giga standard cubic meter (GScm), which is equivalent to 32.87 billion standard cubic feet (BSCF), to 0.96 Giga standard cubic meter (GScm), which is equivalent to 33.93 billion standard cubic feet (BSCF) as a total volume. (Fig. 12).

6.2.2 Inversion Analysis

Following the construction of the initial model, several inversion techniques and inversion analyses were performed. Four distinct inversion analyses were adopted to build the initial impedance models for different types of post-stack inversion, which are classified as mentioned below [60], [61], [62], [63], [64], [65], [66], [67], [68], [69], [70].

This research applied four different inversion techniques for post-stack inversion, as indicated.

- Colored inversion
- Bandlimited inversion
- Maximum Likelihood Sparse Spike inversion
- Model Based inversion

All of these inversion approaches were initially applied to the first AI model and subsequently to the initial elastic impedance. The inversion analysis is done for the interval from 2100 ms to 3000 ms at the Pliocene section for post-stack inversion (Figure 7).

The validity of the inversion outputs was verified using the black-colored seismic stack data in conjunction with the red-colored synthetic data. To achieve this, the blue-colored curve, which represents the original log data, and the red-colored curve, indicating the trajectory of reversed AI, were cross-correlated. The black curve shows how the red and blue colours fit together (Figure 7).

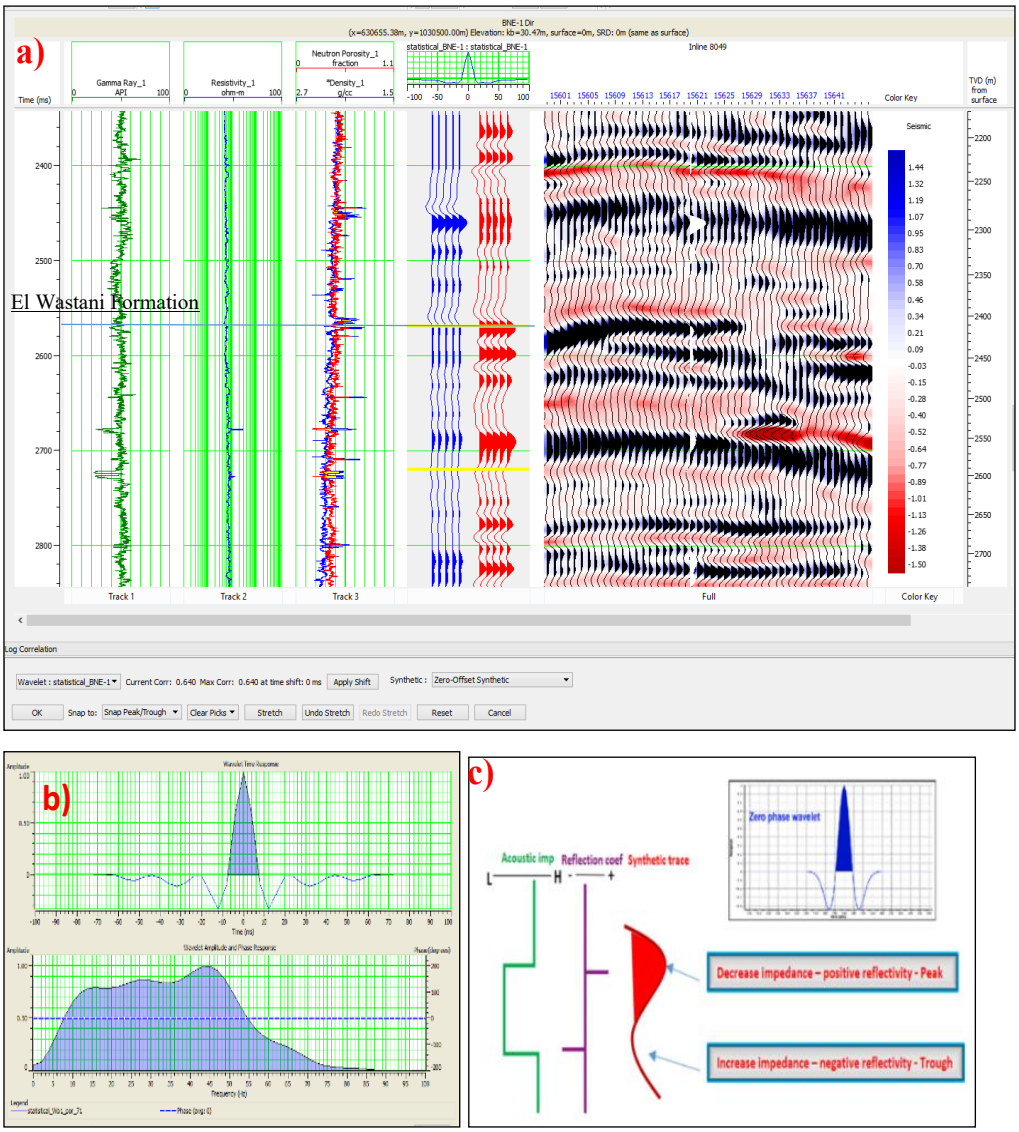

Figure 6: a) Well-seismic correlation for BNE-1 dir well. b) Wavelet statistical properties of BNE-1 dir well. c) Phase characteristics and polarity analysis of BNE-1 dir well."

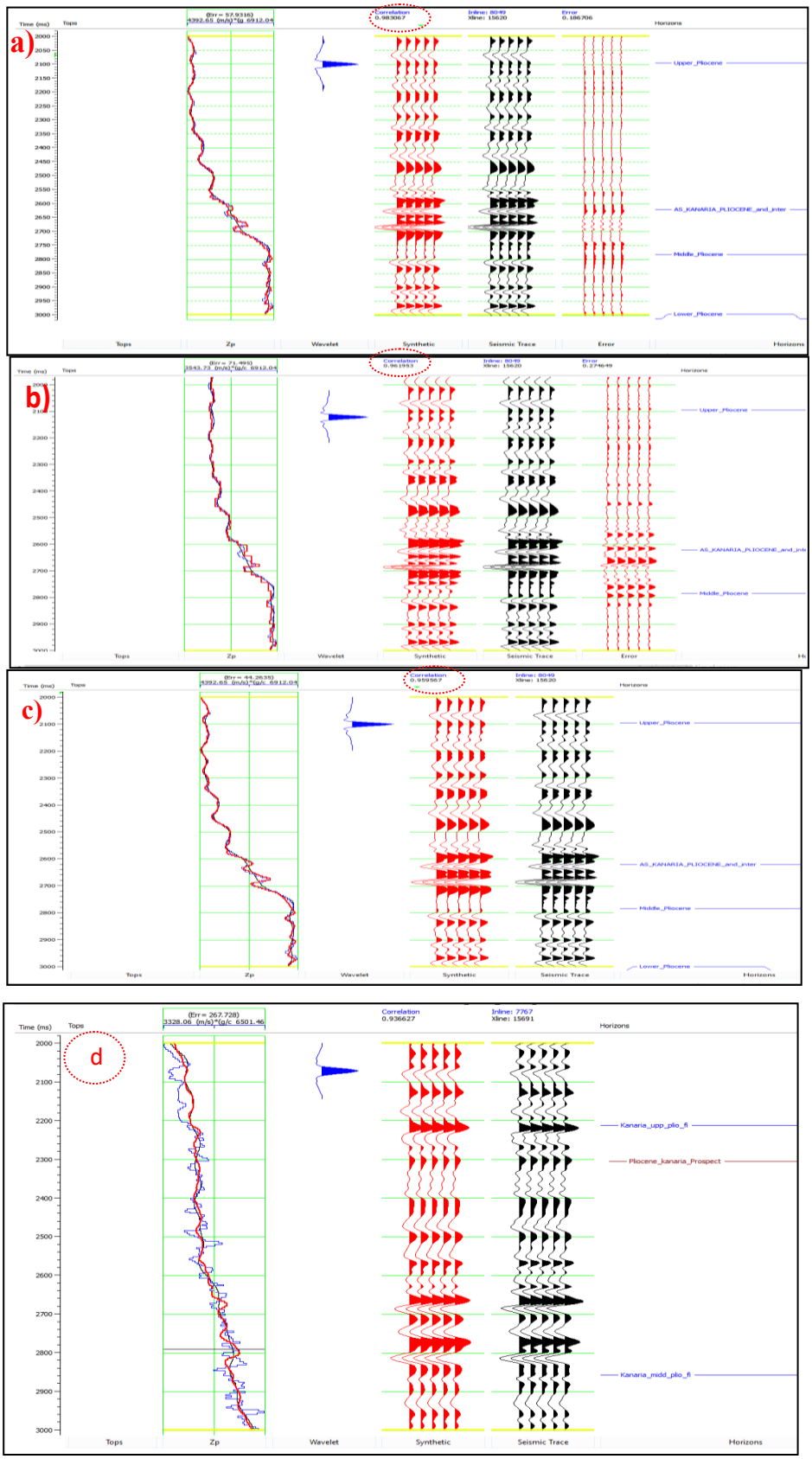

Figure7: a) Color post-stack inversion results for BNE-1 dir well, P.P.A., demonstrating a correlation of roughly 0.98%. b) Band-limited post-stack inversion results for BNE-1 Dir Well, P.P.A., with a correlation of roughly 0.96%. b) Sparse spike post-stack inversion results for BNE-1 dir well, P.P.A., with a correlation of around 0.95%. d) Model-based post-stack inversion results for BNE-1 dir well, P.P.A., with a correlation of roughly 0.93%.

6.3 Post-stack inversion

The calculation of AI volume can be achieved by utilizing seismic data, along with well data and a fundamental stratigraphic interpretation, through the process of inversion. This allows for approximating reservoir characteristics at locations distant from the well. P-impedance (AI) is specially calculated using post-stack seismic inversion and reflection from seismic analysis.

Convolution produces the seismic trace s(t), which is obtained by combining the analysis of the wavelet w(t) and reflectivity series r(t) with an extra disturbance known as n(t). Equation (1) can be used to express how the result was determined mathematically. The equation is illustrated by [14, 48], and has provided evidence for this representation.

$$S(t) = r(t) * w(t) + n(t) \quad \text{, Eq.1}$$

The post-stack AI inversion approach originated at the beginning of the 1980s, when wavelet amplitude and phase spectra extraction methods were widely available. The inversion findings showed excellent resolution, enhanced interpretation, and minimal drilling risk [71].

Post-stack inversion is divided into four main categories:

6.3.1 Colored inversion

Colored inversion uses a specific frequency domain filtering technique to generate reservoir characteristics. This method involves applying a single operator to convert seismic data into an inversion result. Although effective for stratigraphic interpretation and reservoir thickness estimation, it may produce artifacts and requires comprehensive quality control [72], [73].

6.3.2 Sparse-spike inversion

Sparse-spike inversion focuses on large spikes (significant impedance changes) in the seismic data, improving resolution. It blends high-resolution well log data with seismic data and is fast, but may miss small geological features and be sensitive to errors in well logs [74], [75], [76].

6.3.3 Band limited inversion

Band-limited inversion extends sparse-spike inversion by decomposing seismic frequencies to better identify thin layers. It enhances robustness against layer thickness variations but is limited by noise and seismic wavelet characteristics [77].

6.3.4 Model based Inversion

This approach combines seismic data, well logs, and high-frequency geological models to produce a high-resolution impedance cube. Model-based inversion offers the highest resolution but requires more processing time and detailed seismic wavelet data [78], [79], [80], [81], [82].

6.4 Volumetric assessment

The purpose of geological volumetric assessment is to determine the amount of hydrocarbon present within a prospective anomaly based on available seismic interpretation, well log analysis, and finally, seismic inversion, which has a significant role in increasing the total hydrocarbon in place (HIIP), [83], [84], [85].

The volumetric calculation is carried out by Prospect Resources Evaluation by Scenarios software (PRES), which utilizes Monte Carlo simulation to process data, resulting in a numerical model that accurately represents the anticipated or established conditions of the reservoir.

PRES software provides a comprehensive assessment of resources, considering reservoir geometry and numerical models to estimate hydrocarbons. For the Kanaria prospect, six scenarios based on sand facies distribution and geo-body volumes were analyzed. The unrisked resource distribution can be converted to risked resources using the probability of success (POS). PRES generates outputs in numerical and graphical curves, including production profiles with cumulative and probability curves (P10, P50, P90, and mean), referred to as 'risked values,' representing gas initially in place (GIIP).

The goals of volumetric calculation are to estimate hydrocarbon potential for single and multiple targets using available or uncertain data, compute parameters for incomplete thermodynamic and petrophysical data, and enable probability estimates for resource levels. These estimations assist in maximizing predicted resources, supporting exploration programs, and ensuring resource security by storing input/output data in a relational database."

The evaluation of gas Initially in Place (GIIP) has been carried out using the Monte Carlo simulation. The parameters used in gas Initially in Place (GIIP) calculation are summarized for the P.P.A. (K.F. Fm.) at (table 2), by using the petrophysical parameters of the BN-3, BNE-1 dir and ANDALEEB- 1 wells, which encounter P.P.A..
By applying these parameters, the gas Initially in Place (GIIP) after applying seismic inversion to identify the best gas area for the hydrocarbon calculation, which mean gas area increased at the P.P.A. which mean gas area increased from 3.10 Km^2 to 3.68 Km^2, and the mean value of gas Initially in Place (GIIP) changes from around 0.93 Giga standard cubic meter (GScm), which equivalent to 32.87 billion slandered cubic feet (BCF) to 0.96 Giga standard cubic meter (GScm), which equivalent to 33.93 billion standard cubic feet (BSCF) as a total volume. (Figure 12).

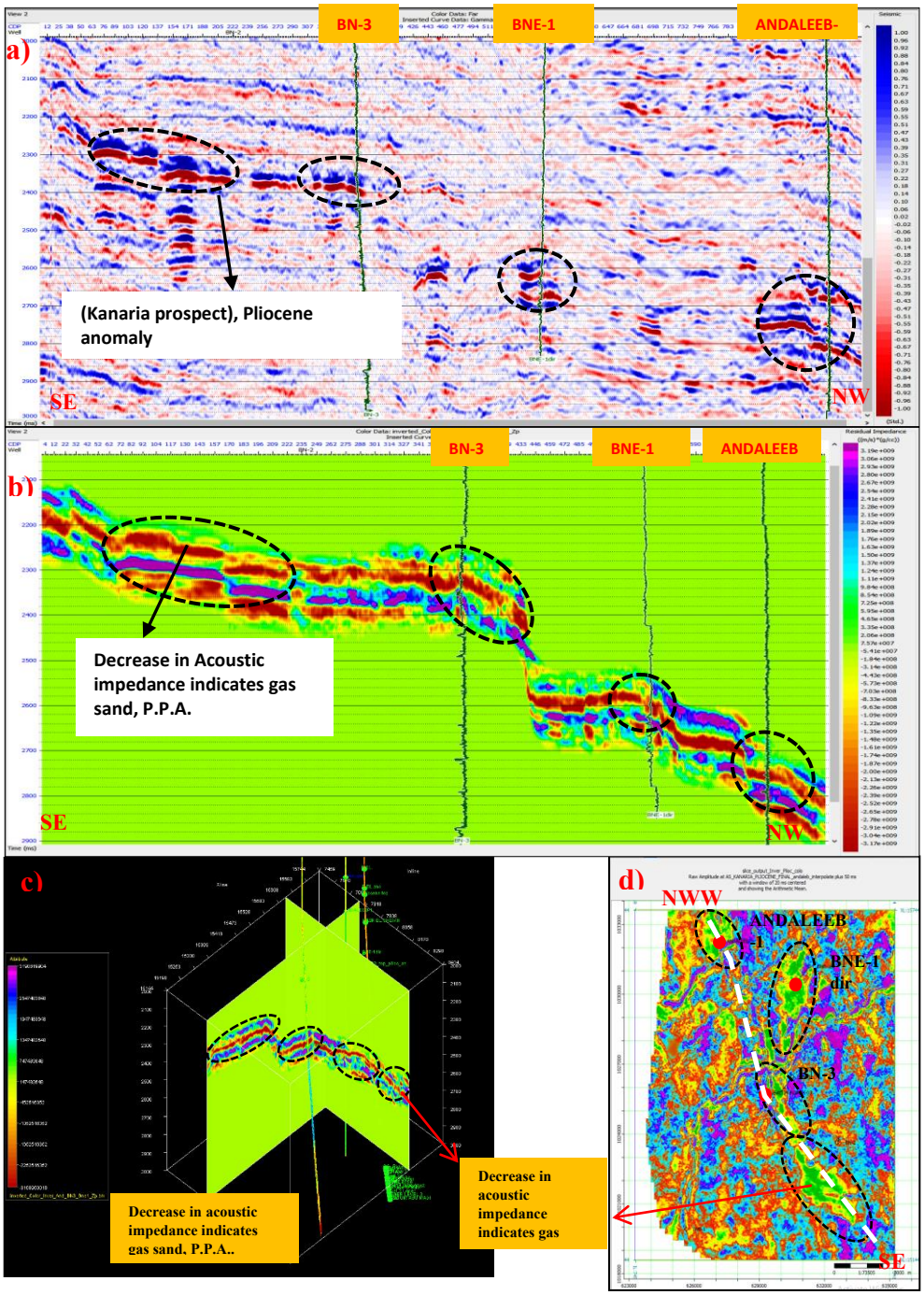

Figure 8: a) Far SW-NE seismic profile at P.P.A. (K.F. Fm.). b) SW-NE seismic profile displaying the colored inversion result, P.P.A. Pliocene anomaly (K.F. Formation). c) 3D view representing colored inversion, P.P.A. Pliocene anomaly (K.F. Formation). d) Time slice derived from the colored inversion, taken from K.F. Formation (P.P.A. Pliocene anomaly.

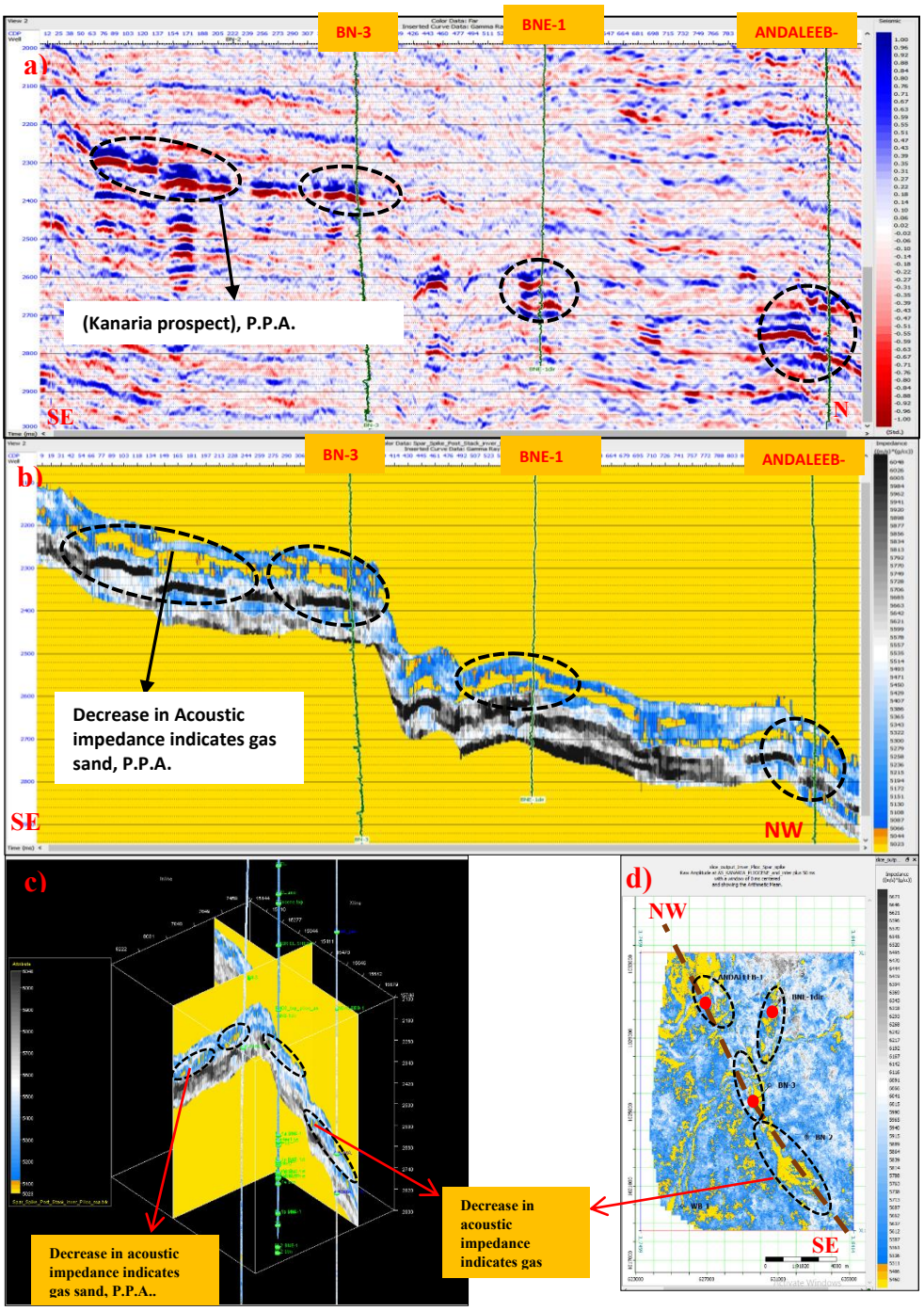

Figure 9: a) Far SW-NE seismic profile at P.P.A. (K.F. Fm.). b) SW-NE seismic profile displaying the Spar spike inversion result, P.P.A. (K.F. Fm.). c) 3D view representing the Spar spike inversion, P.P.A. (K.F. Fm.). d) Time slice taken from the Spar spike inversion, obtained from K.F. Fm. (P.P.A.).

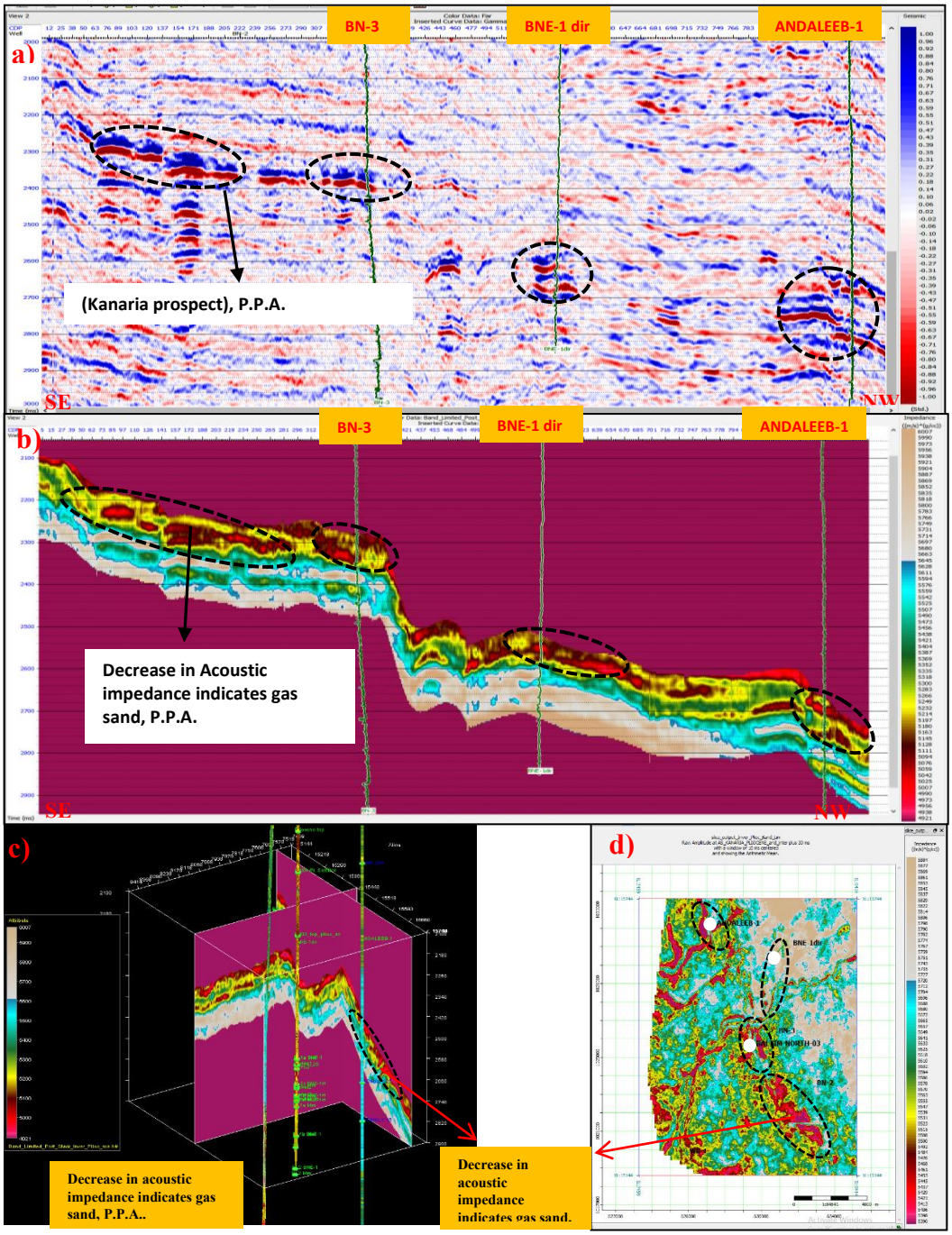

Figure 10: a) Far SW-NE seismic profile at P.P.A. (K.F. Fm.). b) SW-NE seismic profile displaying the colored inversion result, P.P.A. (K.F. Fm.). c) 3D view representing Band Limited inversion, P.P.A. (K.F. Fm.). d) Time slice derived from the Band Limited inversion, obtained from K.F. Fm. (P.P.A.)

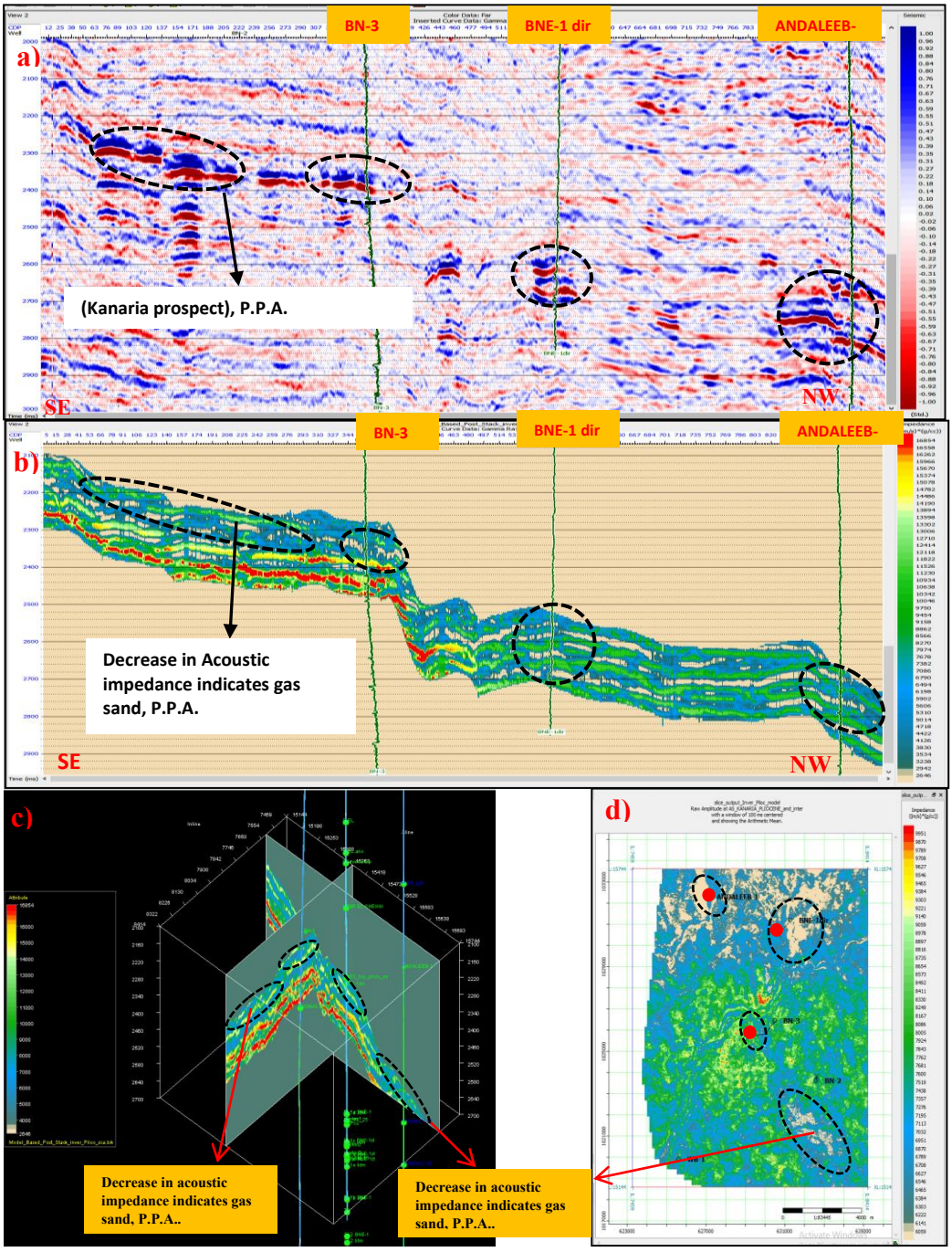

Figure: 11 a) Far SW-NE seismic profile at P.P.A. (K.F. Fm.). b) SW-NE seismic profile. displaying the model-based inversion result, P.P.A. (K.F. Fm.). c) 3D view representing the model-based inversion, P.P.A. (K.F. Fm.). d) Time slice derived from the model-based inversion, obtained from K.F. Fm. (P.P.A.).

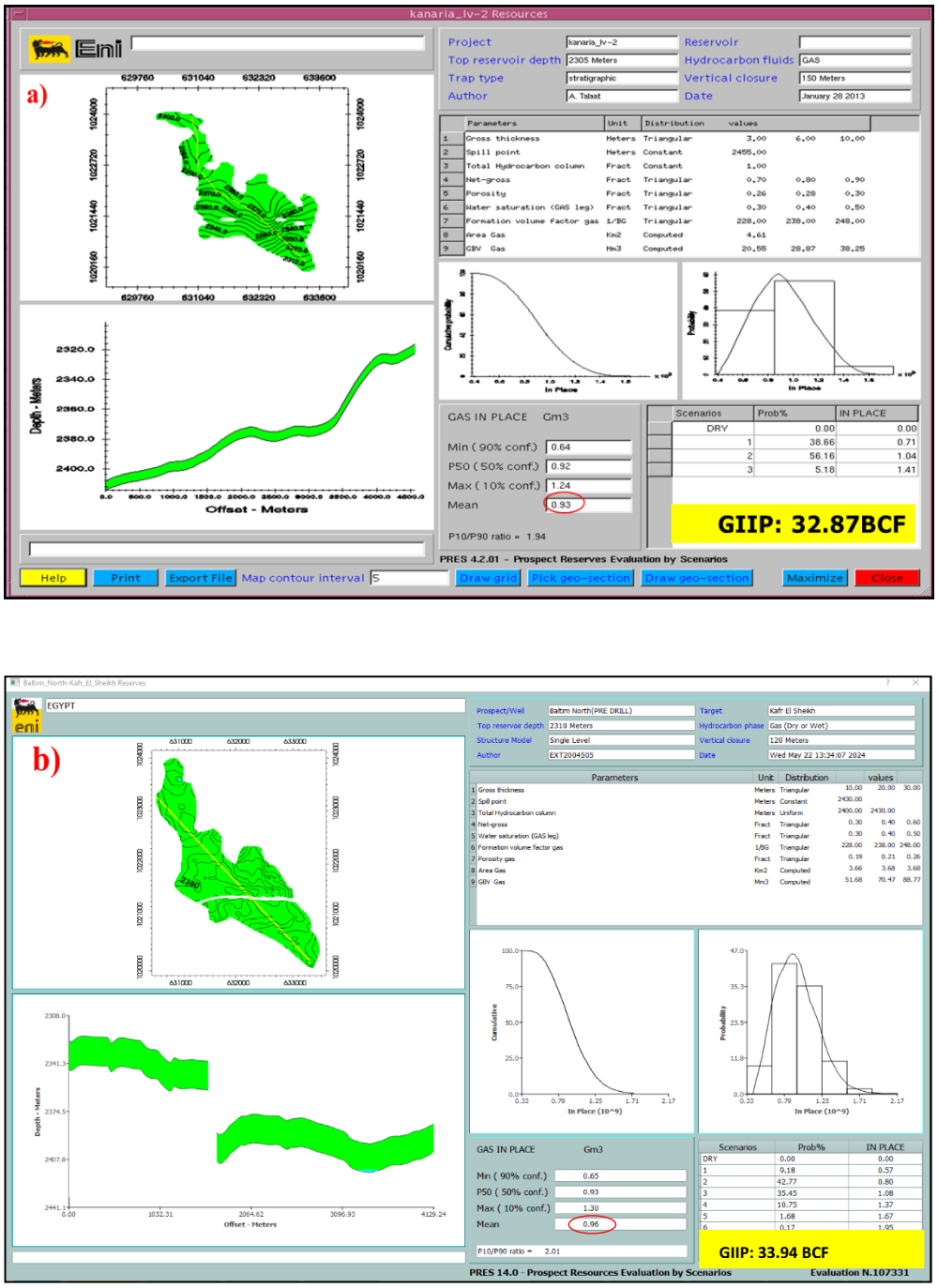

Figure 12: a) Volumetric estimation of the P.P.A. (K.F. Fm.) befor inversion. b) Volumetric estimation of the P.P.A. (K.F. Fm.) after inversion.

7. Conclusion

The main issue, which solved by this study, that, the fake amplitude that can be appeared according to existence of tiny amount of gas which considered not commercial for production, make some restrictions to drill and to avoid any decrease of possibility of drilling success. The basic contribution of the present research is to execute various types of post-stack inversion, specifically colored and band-limited, which give low acoustic impedance at top gas Pliocene reservoir sand and then compare the outcomes with seismic attributes as amplitude attribute, which give high magnitude at far amplitude compared to low magnitude of near amplitude, and give indication for Class III of Amplitude versus Offset (AVO), consequently the value of gas initially in place (GIIP) increased from 32.87 billion standard

cubic feet (BSCF) to 33.94 (BSCF). Subsequently, by implementing various post-stack inversion methods on a seismic cube, distinct seismic inversion cubes are produced. Among these, the color post-stack inversion cube and the band-limited post-stack inversion cube prove to be the most advantageous for estimating gas volume, thereby enhancing the possibility of success for the Pliocene prospect in the Baltim Field Area. This success will encourage additional gas well drilling, leading to increased gas production in the Baltim Field Area.

8. Acknowledgements

The authors wish to extend their gratitude to the Belayim Petroleum Company, the Egyptian General Petroleum Corporation (EGPC), and the Geophysics Department at Cairo University for their support in facilitating this research. .

9. Additional Information

- **Competing interests**

No financial and non-financial competing interests.

- **Data availability**

Data can be requested from Mr. Ali Saeed Ali El-Sayed, the first author of the article; (Email: ayehia2@petrobel.org, aliyehia665@yahoo.com, alisayed@gstd.sci.cu.edu.eg)

References

[1] M. I. Abdel-Fattah and A. Y. Tawfik, 3D Geometric Modeling of the Abu Madi Reservoirs and Its Implication on the Gas Development in Baltim Area (Offshore Nile Delta, Egypt). International Journal of Geophysics, vol. 2015, Article ID 369143, pp. 1–11, 2015.

[2] Othman, A. Bakr, and A. Maher, Integrated Seismic Tools to Delineate Pliocene Gas-Charged Geobody, Offshore West Nile Delta, Egypt. NRIAG Journal of Astronomy and Geophysics, vol. 6, no. 1, pp. 81–89, 2017.

[3] H. El-Mowafy, Gas Sand Detection Using Rock Physics and Pre-Stack Seismic Inversion, Example from Offshore Nile Delta, Egypt. Al-Azhar Bulletin of Science, vol. 27, no. 2-D, pp. 65–72, 2016.

[4] M. A. Sarhan, Assessing Hydrocarbon Prospects in Abu Madi Formation Using Well Logging Data in El-Qara Field, Nile Delta Basin, Egypt. Journal of Petroleum Exploration and Production Technology, vol. 11, no. 6, pp. 2539–2559, 2021.

[5] F. M. El-Fawal, M. A. Sarhan, R. E. L. Collier, A. Basal, and M. H. A. Aal, Sequence Stratigraphic Evolution of the Post-Rift Megasequence in the Northern Part of the Nile Delta Basin, Egypt. Arabian Journal of Geosciences, vol. 9, no. 11, p. 585, 2016.

[6] G. M. Gobashy, A. M. F. Dahroug, A. H. Zakaria, A. M. Salaheldin, and S. M. Sharafeldin, Integrated AVO Inversion and Seismic Attributes for Tracing Hydrocarbon Accumulation in Kafr El-Sheikh Formation, South Batra Field, Nile Delta, Egypt: A Case Study. Contributions to Geophysics and Geodesy, vol. 52, no. 2, pp. 219–234, 2022.

[7] H. Kamel, T. Eita, and M. Sarhan, Nile Delta Hydrocarbon Potentiality, in EGPC. 14th Petroleum Exploration and Production Conference, Cairo, vol. 2, pp. 485–503, 1998.

[8] M. A. Sarhan and M. G. Safa, Application of Seismic Attributes for Detecting Different Geologic Features within Kafr El Sheikh Formation, Temsah Concession, Nile Delta Basin. Scientific Journal of Damietta Faculty of Science (SJDFS), vol. 7, no. 1, pp. 26–34, 2017.

[9] E. Tawadros, Geology of Egypt and Libya, Balkema A., pp. 146–155, 2001.

[10] M. A. Sarhan, Gas-Generative Potential for the Post-Messinian Megasequence of Nile Delta Basin: A Case Study of Tao Field, North Sinai Concession, Egypt, Journal of Petroleum Exploration and Production Technology, vol. 12, no. 4, pp. 925–947, 2021.

[11] M. A. Sarhan, New Prospective Gas Plays in Pliocene Sands, Offshore Nile Delta Basin: A Case Study from Kamose-1 Well at North Sinai Concession, Egypt, Petroleum Research, vol. 7, no. 3, pp. 329–340, 2022.

[12] M. Metwally, W. M. Mabrouk, A. I. Mahmoud, A. Eid, M. M. Amer, and A. M. Noureldin,

Formation Evaluation of Abu Madi Reservoir in Baltim Gas Field, Nile Delta, Using Well Logs, Core Analysis and Pressure Data. Scientific Reports, 2023.

[13] Samuel, S. Kneller, A. S. Raslan, S. A. Andy, and C. Parsons, Prolific Deep-Marine Slope Channels of the Nile Delta, Egypt. AAPG Bulletin, vol. 87, pp. 541–560, 2003.

[14] K. Khaled, G. M. Attia, F. Metwalli, and F. Fagelnour, Subsurface Geology and Petroleum System in the Eastern Offshore Area, Nile Delta, Egypt. SSRN Electronic Journal, 2014.

[15] S. Eze, O. Orji, S. Nnorom, and K. Ubogun, Model-Based Inversion of Acoustic Impedance from Seismic Trace for Lithofacies Differentiation: An Application in Xy Field Offshore Niger Delta. Journal of Applied Sciences and Environmental Management, vol. 23, no. 9, pp. 1677–1684, 2019.

[16] H. Ismail, H. F. Ewida, M. G. Al-Ibiary, and A. Zollo, Integrated Prediction of Deep-Water Gas Channels Using Seismic Colored Inversion and Spectral Decomposition Attribute, West Offshore, Nile Delta, Egypt. NRIAG Journal of Astronomy and Geophysics, vol. 9, no. 1, pp. 459–470, 2020.

[17] H. Mohamed, W. M. Mabrouk, and A. Metwally, Delineation of the Reservoir Petrophysical Parameters from Well Logs Validated by the Core Samples: Case Study Sitra Field, Western Desert, Egypt. J. Afr. Earth Sci., vol. 162, pp. 103754, 2020.

[18] H. Russell, Introduction to Seismic Inversion Methods. Society of Exploration Geophysicists Course Note Series, no. 2, Tulsa, SEG, p. 90, 1988.

[19] Russell and D. Hampson, A Comparison of Post-Stack Seismic Inversion Methods, Ann. Mtg. Abstracts. Society of Exploration Geophysicists, pp. 876–878, 1991.

[20] Othman, F. Metwaly, M. Fathy, and A. Salama, Use of PNN and Post Stack Inversion to Predict Reservoir Characterization in the Mediterranean Sea, Egypt. Sapphire Field, 2022.

[21] Abdel Aal, R. J. Price, J. D. Vaital, and J. A. Shrallow, Tectonic Evolution of Nile Delta, Its Impact on Sedimentation and Hydrocarbon Potential, in EGPC, 12th Petrol. Expl. Prod. Conf., Cairo, vol. 1, pp. 19–34, 1994.

[22] S. Hemdan and J. M. Jonathan, Nile Delta Gas Origin and Biogenic Gas Potential, MOC, 2008.

[23] Abdel Aal, A. El Barkooky, M. Gerrits, H. Meyer, M. Schwander, and H. Zaki, Tectonic Evolution of the Eastern Mediterranean Basin and Its Significance for Hydrocarbon Prospectivity in Ultra-Deep Water of the Nile Delta, The Leading Edge, vol. 19, pp. 1041–1152, 2000.

[24] P. M. Barber, Messinian Subaerial Erosion of the Proto Nile Delta, Marine Geology, vol. 44, pp. 253–272, 1981.

[25] Dolson, J., The Petroleum Geology of Egypt and History of Exploration, Regional Geology Reviews, pp. 635–658, 2019.

[26] J. C. Harms and J. I. Wray, Nile Delta, Balkema, AA, Rotterdam, Netherlands, p. 743, 1990.

[27] E. R. Orwig, Tectonic Framework of Northern Egypt and the Eastern Mediterranean Regime, in EGPC 6th Exploration Seminar, Cairo, Egypt, p. 20, 1982.

[28] R. Salem, Evolution of Eocene-Miocene Sedimentation Patterns in Parts of Northern Egypt, AAPG Bulletin, vol. 60(1), pp. 34–64, 1976.

[29] Sarhan, M., and Hemdan, K., North Nile Delta Structural Setting and Trapping Mechanism, Egypt, in EGPC, 12th Petrol. Exp. Prod. Conf., Cairo, vol. 1, pp. 1–18, 1994.

[30] A. Rizzini, F. Vezzani, V. Cococcetta, and G. Milad, Stratigraphy and Sedimentation of a Neogene-Quaternary Section in the Nile Delta Area (A.R.E.), Marine Geology, vol. 27, pp. 327–348, 1978.

[31] Sestini, G., Nile Delta: A review of depositional environments and geological history. edited by Whiteley, M. K., and Pickering, K., in Delta Sites and Traps for Fossil Fuels, Geological Society Special Publication 41, pp. 99–127, 1989.

[32] Doherty, M., Jamieson, G., Kilanyi, T., and Trayner, P., The geology and seismic stratigraphy of the offshore Nile Delta, Egypt. in EGPC, 9th Exploration and Production Conference, vol. 2, pp. 408–425, 1988.

[33] Maguire, D., El Fattah, A., Seligmann, P., and Duncan, D., Pliocene slope channel architecture in West Med as driven by shallow seismic analogs. MOC, 2008.

[34] Nini, C., Checchi, F., El Blasy, A., and Talaat, A., Depositional evolution of the Plio-Pleistocene succession as a key for unraveling the exploration potential of the post-Messinian play in the Central Nile Delta. MOC, Nazmul Haque, 2010.

[35] Tawadros, E., Geology of Egypt and Libya, Balkema, A., pp. 146–155, 2001.
[36] Ali, A., Alves, T. M., Saad, F. A., Ullah, M., Toqeer, M., and Hussain, M., Resource potential of gas reservoirs in South Pakistan and adjacent Indian subcontinent revealed by post-stack inversion techniques. Journal of Natural Gas Science and Engineering, vol. 49, pp. 41–55, 2018.
[37] Datta Gupta, S., Sinha, S. K., and Chahal, R., Capture the variation of acoustic impedance property in the Jaisalmer Formation due to structural deformation based on post-stack seismic inversion study: A case study from Jaisalmer sub-basin, India, Journal of Petroleum Exploration and Production Technology, vol. 12(7), pp. 1919–1943, 2022.
[38] Castagna, J. P., Sun, S., and Siegfried, R. W., Instantaneous spectral analysis: detection of low-frequency shadows associated with hydrocarbons. The Leading Edge, vol. 22, pp. 120–127, 2003.
[39] Peyton, L., Bottjer, R., and Partyka, G., Interpretation of incised valleys using new 3-D seismic techniques: A case history using spectral decomposition and coherency. The Geophysics, vol. 70, pp. 19–25, 1998.
[40] Dewan, J. T., Essentials of Modern Open-Hole Log Interpretation. PennWell Publ. Co., Tulsa, Oklahoma, 361 pp, 1983.
[41] Mohamed, H., Mabrouk, W. M., Metwally, A., Delineation of the reservoir petrophysical parameters from well logs validated by the core samples case study Sitra field, Western Desert, Egypt. Scientific Reports, vol. 14(1), 26841, 2024.
[42] S. El-Sayed, W. M. Mabrouk, and A. M. Metwally, Utilizing post-stack seismic inversion for delineation of gas-bearing sand in a Pleistocene reservoir, Baltim Gas Field, Nile Delta, Egypt. Scientific Reports, 2024.
[43] K. J. Weber, Hydrocarbon distribution patterns in Nigerian growth-fault structures controlled by structural style and stratigraphy: ABSTRACT, AAPG Bulletin, vol. 70, 1986.
[44] T. B. Berge, F. Aminzadeh, P. D. Groot, and T. Oldenziel, Seismic inversion successfully predicts reservoir, porosity, and gas content in Ibhubesi field, Orange Basin, South Africa. Leading Edge, vol. 21, pp. 338–348, 2002.
[45] A. M. Al-Rahim and H. A. Hashem, Subsurface 3D prediction porosity model from converted seismic and well data using model-based inversion technique. Iraqi J. Sci., vol. 57, no. 1A, pp. 163-174, Jan. 2016.
[46] J. C. Glorioso and A. Rattia, Unconventional reservoirs: basic petrophysical concepts for shale gas, All Days, 2012.
[47] O. Fajana, M. A. Ayuk, P. A. Enikanselu, and A. R. Oyebamiji, Seismic interpretation and petrophysical analysis for hydrocarbon resource evaluation of 'Pennay' field, Niger Delta. Journal of Petroleum Exploration and Production Technology, vol. 9(2), pp. 1025–1040, 2018.
[48] T. Muther, H. A. Qureshi, F. I. Syed, H. Aziz, A. Siyal, A. K. Dahaghi, and S. Negahban, Unconventional hydrocarbon resources: geological statistics, petrophysical characterization, and field development strategies. J. Pet. Explor. Prod. Technol., vol. 12, no. 6, pp. 1463-1488, Dec. 2021.
[49] Y. Zhang, Z. Li, Y. Li, and X. Zhang, Challenges and countermeasures of log evaluation in unconventional petroleum exploration and development. Pet. Explor. Dev., vol. 48, no. 5, pp. 1033-1047, Oct. 2021.
[50] Hesham, N. A. Fattah, and A. Dahroug, Integrating seismic attributes and rock physics for delineating Pliocene reservoir in Disouq field, Nile Delta, Egypt. Contributions to Geophysics and Geodesy, vol. 53(1), pp. 65–84, 2023.
[51] M. L. Greenberg and J. P. Castagna, Shear-wave velocity estimation in porous rocks: Theoretical formulation, preliminary verification, and applications. Geophysical Prospecting, vol. 40, pp. 195–209, 1992.
[52] S. Jalal, H. Rehman, S. U. Alam, and A. Wahid, Estimation of reservoir porosity using seismic post-stack inversion in Lower Indus Basin, Pakistan. International Journal of Economic and Environmental Geology, vol. 12(2), pp. 60–64, 2023.
[53] J. R. Krebs, J. E. Anderson, D. Hinkley, R. Neelamani, S. Lee, A. Baumstein, and M.-D. Lacasse, Fast full wave seismic inversion using encoded sources. Geophysics, vol. 74, pp. 177–188, 2009.
[54] N. Mondol, From sedimentary environments to rock physics. Petroleum Geosciences, Springer,

Berlin, 381 pp, 2010.
[55] Hashem, A. E. N. Helal, and A. M. S. Lala, Application of AVO and seismic attributes techniques for characterizing Pliocene sand reservoirs in Darfeel field, Eastern Mediterranean, Egypt. International Journal of Geosciences, vol. 13(10), pp. 973–984, 2022.
[56] Ismail, H. F. Ewida, M. G. Al-Ibiary, and A. Zollo, Application of AVO attributes for gas channels identification, West offshore Nile Delta, Egypt. Petroleum Research, vol. 5, no. 2, pp. 112–123, 2020.
[57] A.S.A. Majeed and K.K. Ali, 3D Seismic Structural Study of Zubair Formation in Najaf-Karbala Area-Central Iraq. Iraqi Journal of Science, pp. 2342-2353, 2023.
[58] K.K. Ali and G.F. Kadhim, 3D seismic attributes interpretation of Zubair Formation in Al-Akhaideir area, Southwestern Karbala. The Iraqi Geological Journal, pp. 17-25, 2020.
[59] B.S. Al-Azzawi and K.K. Ali, 2D Seismic Structural Study of the Area Between Halfaya, Noor and Amara Oil Fields, Southeastern Iraq. Iraqi Journal of Science, 65(7), pp. 3812–3823, 2024.
[60] Y. Zhao et al., Seismic inversion for high-resolution subsurface property estimation: A comparison of techniques. Journal of Geophysics and Engineering, vol. 20, no. 1, pp. 54–67, 2023.

[61] M. Hussein, A. Abu El-Ata, and M. El-Behiry, AVO analysis aids in differentiation between false and true amplitude responses: A case study of El Mansoura field, onshore Nile Delta, Egypt. J. Pet. Explor. Prod. Technol., pp. 969–989, 2019.
[62] X. Li and X. Xie, A fast seismic inversion algorithm based on least-squares reverse time migration. Geophysical Prospecting, vol. 72, no. 4, pp. 810–825, 2024.
[63] O. Rashad, A. El-Barkooky, A. El-Araby, and M. El-Tonbary, Deterministic and Stochastic Seismic Inversion techniques towards a better prediction for the reservoir distribution in NEAG-2 Field, North Western Desert, Egypt. Egyptian Journal of Petroleum, vol. 31, no. 1, pp. 15–23, 2022.
[64] P. C. H. Veeken and M. Da Silva, Seismic inversion methods and some of their constraints. First Break, vol. 22, pp. 47–70, 2004.
[65] P. C. H. Veeken and M. Rauch-Davies, AVOS attribute analysis and seismic reservoir characterization. First Break, vol. 24, pp. 41–52, 2006.
[66] T. Ferreirinha, R. Nunes, L. Azevedo, A. Soares, F. Pratas, P. Tomás, and N. Roma, Acceleration of stochastic seismic inversion in OpenCL-based heterogeneous platforms. Comput. Geosci., vol. 78, pp. 26–36, 2015.
[67] Y. Wang, Seismic Inversion: Theory and Applications. Wiley Blackwell, Nov. 2016.
[68] L. Krischer, A. Fichtner, S. Simute, and H. Igel, Large-scale seismic inversion framework. Seismol. Res. Lett., vol. 86, no. 4, pp. 1198–1207, Jun. 2015.
[69] O. S. Doohee and A. M. Al-Rahim, Enhancement of seismic reflectors by using VSP and seismic inversion in Sindbad oil field, south of Iraq. Iraqi J. Sci., vol. 59, no. 3C, 2018.
[70] A. K. Jaheed and H. H. Karim, Implementation of seismic inversion to determine porosity distribution of Maysan in Amara oil field, southern Iraq. Iraqi J. Sci., vol. 63, no. 7, 2022.
[71] O. S. Doohee and A. M. Al-Rahim, Enhancement of seismic reflectors by using VSP and seismic inversion in Sindbad oil field, south of Iraq. Iraqi J. Sci., vol. 59, no. 3C, 2018.
[72] J. Fatti et al., Pre-stack and post-stack inversion: Advancements in seismic interpretation methods. Journal of Geophysics, vol. 71, no. 4, pp. 55–78, 2006.
[73] D. P. Hampson, J. S. Schuelke, and J. A. Quirein, Use of multi-attribute transforms to predict log properties from seismic data. Geophysics, vol. 66, no. 1, pp. 220–236, 2000.
[74] S. P. Maurya and K. H. Singh, Predicting Porosity by Multivariate Regression and Probabilistic Neural Network using Model-based and Coloured Inversion as External Attributes: A Quantitative Comparison. Journal of the Geological Society of India, vol. 93, no. 2, pp. 207–212, 2019.
[75] S. Singh, A. I. Kanli, and S. Sevgen, A general approach for porosity estimation using artificial neural network method: A case study from Kansas gas field. Stud. Geophys. Geod., vol. 60, no. 1, pp. 130–140, 2016.
[76] W. Chen et al., Deep learning vertical resolution enhancement considering features of seismic data. IEEE Journals & Magazine, 2024.

[77] B. Morozov and J. Ma, Accurate poststack acoustic-impedance inversion by well-log calibration. Geophysics, vol. 74, no. 5, pp. R59–R67, 2009.
[78] Assad, A Petroleum Geologist's Guide to Seismic Reflection. Wiley–Blackwell, 2012.
[79] S. U. Karim, M. S. Islam, M. M. Hossain, and M. A. Islam, Seismic Reservoir Characterization Using Model Based Post-Stack Seismic Inversion: In Case of Fenchuganj Gas Field, Bangladesh. Journal of the Japan Petroleum Institute, vol. 59, no. 6, pp. 283–292, 2016.
[80] T. B. Nainggolan, M. P. Adhar, and I. Setiadi, Integration of Post-Stack Inversion and Rock Physics to Determine Sandstone Reservoir Quality: Barakan Sub-basin case. IOP Conference Series: Earth and Environmental Science, vol. 873, no. 1, 012020, 2021.
[81] J. Wang et al., Seismic impedance inversion using a model-based approach and deep learning techniques. Journal of Applied Geophysics, vol. 189, 104443, 2022.
[82] M. Toqeer, A. Ali, T. M. Alves, A. Khan, Zubair, and M. Hussain, Application of model based post-stack inversion in the characterization of reservoir sands containing porous, tight and mixed facies: A case study from the Central Indus Basin, Pakistan. Journal of Earth System Science, vol. 130, no. 2, 2021.
[83] W. Krokstad and Ø. Sylta, Risk assessment using volumetrics from secondary migration modelling: assessing uncertainties in source rock yields and trapped hydrocarbons. in Norwegian Petroleum Society Special Publication, vol. NPF, pp. 219–235, 1996.
[84] P. Gristo, B. Conti, P. Rodríguez, R. Novo, J. Marmisolle, and H. de Santa Ana, Volumetric Assessment of Oil and Gas Prospective Resources in the Offshore of Uruguay. 11° Congreso de Exploración y Desarrollo de Hidrocarburos (Conexplo), 8–11 Noviembre, Mendoza, Argentina, 2022.
[85] M. V. Kok, E. Kaya, and S. Akin, Monte Carlo Simulation of Oil Fields, Energy Sources, Part B: Economics, Planning, and Policy, vol. 1, no. 2, pp. 207–211, 2006.